Mean free path of inelastic electron scattering in elemental solids and oxides using transmission electron microscopy: Atomic number dependent oscillatory behavior

Konstantin Iakoubovskii* and Kazutaka Mitsuishi
Quantum Dot Research Center, National Institute for Materials Science, 3-13 Sakura, Tsukuba 305-0005, Japan

Yoshiko Nakayama and Kazuo Furuya
High Voltage Microscopy Station, National Institute for Materials Science, 3-13 Sakura, Tsukuba 305-0005, Japan
(Received 7 January 2008; revised manuscript received 6 February 2008; published 5 March 2008)

Mean free path of inelastic electron scattering λ has been measured with a 200 keV transmission electron microscope for the majority of stable elemental solids and their oxides. An oscillating behavior vs atomic number Z has been revealed, such that within one row of the Periodic Table, the minimum (maximum) of λ is observed for elements with completed (empty) outer d shells. A significantly weaker $\lambda(Z)$ dependence is observed for the oxides. The $\lambda(Z)$ variation is ascribed to the three major factors: atomic density, number of "free" electrons per atom, and contribution of atomic core-loss transitions.

DOI: 10.1103/PhysRevB.77.104102 PACS number(s): 79.20.Uv, 68.37.Lp, 72.15.Lh, 61.85.+p

I. INTRODUCTION

Inelastic electron scattering has been a subject of numerous studies and reviews (see, e.g., Refs. 1–7). Here, we shall mostly focus on scattering by single atoms and elemental solids. The characteristic measures of the scattering are the cross section σ or mean free path λ. By definition, they are related through the number of atoms N per unit volume as $1/\lambda = N\sigma$ and thus will be used in this paper interchangeably. Those λ (or σ) values are important for a wide range of sciences from radiation physics to transmission electron microscopy (TEM) and are crucial for quantitative analysis of results obtained with various electron spectroscopies. They depend on several experimental parameters, such as electron energy and geometry of the illumination and collection optics. Those dependences have been discussed previously,[1,3,8] and in this paper, we shall analyze variation of λ with the atomic number Z.

Two major $\lambda(Z)$ behaviors are known: periodic oscillation and smooth increase approximated as $1/\lambda = N\sigma \sim Z^a$. Early theories of *atomic* scattering predicted the latter dependence with $a=1/3$ (Ref. 6) or $a=1/2$.[7] However, it was soon realized that this monotonic increase originates from oversimplifications and that more rigorous approach reveals periodic dependence.[5] The latter can be described as follows:[1] Within one row of the Periodic Table, σ decreases from alkali toward noble gases. In the alkali, the valence electrons are rather delocalized and thus produce low-energy scattering spectra, while the noble gases have rather compact, filled s and p shells and therefore high-energy electron loss transitions. The scattering intensity rapidly decreases with energy that results in the above-mentioned σ decrease.

While the $\lambda(Z)$ dependence for atoms is well established, the situation in solids is rather uncertain. The crucial difference in the inelastic electron scattering by atoms and solids is that in atoms, electrons are localized and the scattering originates from electronic transitions between different atomic levels called "core-loss" transitions. The latter are also observed in solids, however, the crucial difference is that in solids, valence electrons are delocalized and produce collective excitations called plasmons. Compared to most core-loss transitions, plasmons have significantly lower energies and higher scattering probabilities. As a result, experimental electron energy loss spectra (EELSs) from most materials are dominated by plasmon excitations. Therefore, it is argued that the atomic calculations are inapplicable to solids,[3,4] and other theoretical approaches are considered.

The most popular one is based on the free-electron (or "jellium") model. When the width of the plasmon peak is small compared to its energy E_p, this model predicts the following relations:

$$1/\lambda = N\sigma \sim E_p \sim n^{1/2} \sim (\rho z/A)^{1/2}. \quad (1)$$

Here, n is the number of free electrons per unit volume, z is number of free electrons per atom, ρ is mass density, and A is atomic mass. Note that (1) we have focused only on Z dependence and thus omitted proportionality constants. (2) The E_p term should actually read $E_p \ln(B/E_p)$, where B is a constant and the logarithmic term originates from angular dependence of the scattering. However, for typical collection angles of >1 mrad, $B/E_p \gg 1$. Therefore, the logarithm is a slow function of E_p, and, considering the experimental errors, it can well be assumed constant. (3) Equation (1), due to the specific $\rho(Z)z(Z)$ dependence, actually does predict periodic $\sigma(Z)$ behavior.

Numerous modifications of the free-electron model exist.[3] The weakness of most of them is uncertain value of z, which is usually taken as the most probable valence that a certain atom exhibits in chemical compounds.

In a striking contrast to a vast number of theoretical studies, systematical measurements of $\sigma(Z)$ are scarce. Egerton[1] summarized λ values for 17 elemental solids and compounds. Despite significant data scatter, the $\lambda(Z)$ dependence was approximated by a smooth $1/\lambda \sim Z^{0.36}$ increase. Yet in another EEL study,[9] data for six solids were fitted with a $1/\lambda \sim Z^{0.57}$ function.

Instead of using *electron* scattering for measuring λ, *optical* absorption has also been employed, assuming the equivalence of those methods for small scattering angles.

Within this approach, σ has been calculated for 34 elemental solids.[4] Again, despite a large scatter, results were approximated by a $1/\lambda \sim Z^{0.5}$ law.

This brief discussion of the material dependence of inelastic scattering can be summarized as follows: Calculations on isolated atoms and solids predict periodic $\sigma(Z)$ or $\lambda(Z)$ behavior, however, it has not been revealed by the experiment. This apparent contradiction is resolved in the present study. By improving the experimental accuracy and increasing the range of studied materials, we reveal a clear periodic behavior of the inelastic mean free path in elemental solids.

II. EXPERIMENTAL DETAILS

The mean free path values were deduced from electron energy loss (EEL) spectra measured with a Jeol 200 kV high vacuum 2500SES scanning transmission electron microscope (STEM) equipped with an Enfina EEL spectrometer. Same microscope was used for recording STEM images. The excitation and collection semiangles were set to ~20 mrad.

Previous studies[1,4] indicated that variation of λ with atomic number is rather small (~100% for the whole Z range), and therefore its reliable measurement requires improved accuracy. This was achieved in the following way.

(1) All measurements were performed at nominally the same microscope settings, without major microscope realignment in between.

(2) Diffraction effects can modulate the EELS intensity and thus result in overestimation of λ by up to 25%.[10] Those effects were minimized by selecting appropriate sample orientation.

(3) Under electron irradiation, TEM samples often rapidly accumulate carbon-related contamination affecting the λ measurements. Using high vacuum ($\sim 10^{-6}$ Pa) and short acquisition time (~50 ms) minimized this problem in the present study. Rapid measurement also allowed us to study materials unstable under focused electron beam such as sulfur, phosphorus, iodine, and some oxides.

(4) Moderately thin sample regions have been chosen ($t/\lambda \sim 1$ or $70 < t < 180$ nm) in order to reduce the surface plasmon contributions, which are non-negligible at small thicknesses t and plural scattering gaining at large thicknesses.[1]

(5) The λ value for a certain material was typically extracted from a single EEL spectrum. Note that usually an extra independent measurement(s) (of thickness, for example) is required. In those additional measurements, it is difficult to precisely locate the sample area used for the EEL spectra. This difficulty probably reduced the accuracy of many previous mean free path measurements.

The following procedure has been applied to deduce the λ values.[8] The EEL spectrum $J(E)$ was deconvoluted with the standard routines[1] to extract the integrated zero-loss peak I_0 and the single-scattering EEL spectrum $S(E)$. The λ values were calculated as

$$\lambda = \frac{t}{\ln(I/I_0)}, \tag{2}$$

where $I = \int J(E)dE$. This equation is derived[1] using the only assumption of independence of electron scattering events (Poisson statistics) and therefore is rather reliable. The sample thickness t was deduced from the same spectrum using the "Kramers-Kronig sum rule,"[1,8,10,11]

$$t = \frac{4a_0 F E_0}{I_0(1 - 1/n^2)} \int \frac{S(E)dE}{E \ln(1 + \beta^2/\theta^2)}. \tag{3}$$

Here, a_0 is the Bohr radius, E_0 is the electron energy, F is the relativistic factor, n is the optical refractive index, β is the collection angle, and $\theta \cong E/(2FE_0)$. This equation is deduced with more approximations than Eq. (2), but several experimental tests[8,10,11] revealed that it is accurate to ~10%.

For many materials, a newly developed[8] and even more accurate routine has been applied: Several layered structures $Si/SiO_2/Ta/CoO/Pt$, $Si/SiO_2/Ta/Pt/NiO/Al$, $Si/SiO_2/Cr/Pt/W$, Si/Au, and Si/diamond were prepared using conventional techniques of magnetron sputtering, thermal evaporation, and chemical vapor deposition. Cross-sectional TEM samples were prepared from those structures by focused ion-beam cutting (Ga^+, 5–30 keV). Ion-beam cutting produced samples with uniform, almost constant, thickness profile, thus avoiding abrupt thickness variation at the interfaces common for most other sample preparation techniques.

EEL spectra from those multilayered samples were automatically acquired at several hundred locations on a straight line running through all the layers. The thus obtained data arrays were processed with Eq. (2) yielding a line profile of relative λ values for several materials. It showed abrupt jumps at the material interfaces superimposed on a slow background originating from minor thickness variations in the studied sample. The latter contribution has been fitted by a second-order polynomial and removed resulting in a corrected line profile of relative λ values. They were converted into absolute ones using the well-calibrated $\lambda = 145$ nm value for crystalline Si.[8,12–15] It is important to note that similar (within 10%) λ values were obtained for those layered structures using Eq. (3) thus confirming the reliability of the Kramers–Kronig sum method.

III. EXPERIMENTAL RESULTS

A. Material dependence of inelastic scattering

Figure 1 summarizes inverse λ values measured at 200 keV for the majority of stable (ambient conditions) elemental solids and oxides. Preliminary results revealed no significant effect of crystalline structure, such that λ values varied within 10% among single crystal, polycrystalline, and amorphous forms. The largest variation was observed for oxides of light elements, such as SiO_2, Al_2O_3, and B_2O_3: λ for amorphous phase was ~10% larger than for the crystalline. We attribute this effect to the smaller mass density common for amorphous phases of many materials. Therefore, single crystalline regions were selected for all the measurements.

Figure 1 reveals a clear periodic dependence of λ such that within one row of the Periodic Table, the minimum (maximum) of λ is observed for elements with completed (empty) outer d shell. A smaller variation is observed for the oxides.

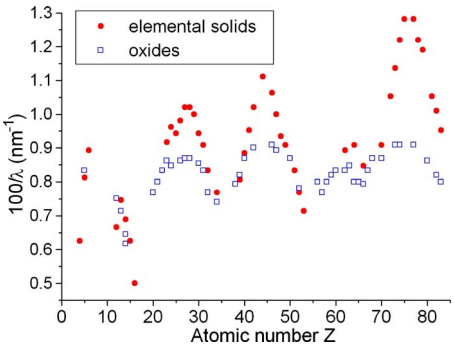

FIG. 1. (Color online) Variation of inverse mean free path of inelastic electron (200 keV) scattering with atomic number Z measured in stable elemental solids and oxides. For oxides, Z corresponds to the main element, e.g., $Z=14$ for SiO_2.

B. Importance of $\lambda(Z)$ dependence for electron microscopy

Note that the revealed above periodic $\lambda(Z)$ behavior has not only academic but also practical value. Apart from the mentioned significance for the various electron spectroscopies and radiation physics, it is also important for the interpretation of TEM images. For example, much of transmission electron microscopy is based on intuitive analysis of the so-called dark-field and bright-field images. Roughly speaking, dark-field images are constructed using electrons scattered at relatively large ($\geqslant$30 mrad for STEM) angles and are dominated by elastic and thermal diffuse scattering. Meanwhile, bright-field pictures are usually obtained at smaller angles and contain a mixture of elastic, thermal diffuse, and inelastic scattering. When sample thickness exceeds few inelastic mean free paths (few hundreds of nanometers), the latter contribution dominates.

Conventional intuitive analysis of dark-field and bright-field TEM images is based on the monotonic increase of $\sigma(Z)$, which is experimentally established for thermal diffuse and elastic[1] and assumed for inelastic scattering (see Introduction). Therefore, *in the absence of diffraction effects*, darker (lighter) areas in bright-field (dark-field) images, respectively, are associated with heavier elements, as shown in panels (a) and (b) of Fig. 2 for a Pt/Cr interface. However,

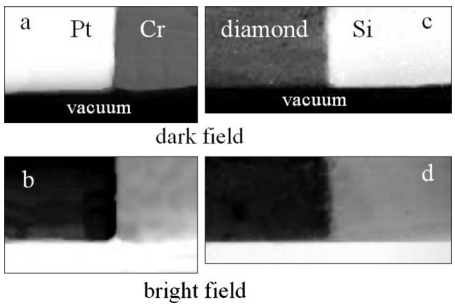

FIG. 2. [(a) and (c)] Dark-field and [(b) and (d)] bright-field STEM images from [(a) and (b)] Pt/Cr and [(c) and (d)] diamond/Si interfaces. Note a usual contrast reversal between dark-field and bright-field images for Pt/Cr. This, however, does not occur in the diamond/Si sample because of "abnormal" λ behavior.

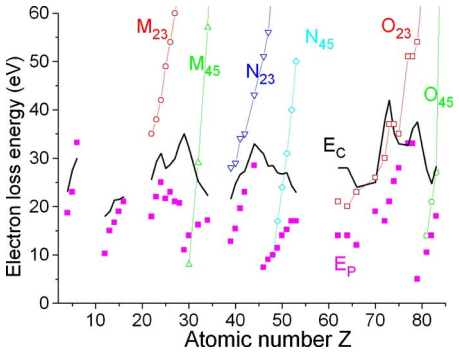

FIG. 3. (Color online) Energies of the core-loss (open symbols) and plasmon (E_P, solid squares) transitions and a characteristic EEL energy E_C (black solid line) (see text for details).

the oscillatory behavior of inelastic scattering revealed in Fig. 1 suggests that caution should be exercised when using this interpretation. Indeed, a solid composed of element with larger Z (i.e., *stronger* elastic and thermal diffuse scattering) can have smaller $1/\lambda$ value (i.e., *weaker* inelastic scattering). An illustrative example is the bright- and dark-field pictures of a technologically important diamond/Si interface shown in Figs. 2(c) and 2(d). A thick sample has been selected for this demonstration such that the (multiple) inelastic events dominated the scattering. Note that here diamond area appears darker than Si both in dark- and bright-field pictures. This could cause misinterpretations of bright-field images of mixed-phase samples where the spatial distribution of different materials is unknown.

It is important to stress that the contrast of the bright-field images can also be altered by diffraction effects and that the above example merely demonstrates that if those effects are experimentally avoided or negligible (e.g., in amorphous or fine-grain solids), then the material dependence of inelastic scattering must be taken into account. As to Fig. 2, the Pt, Cr, and diamond areas have indeed fine-grain polycrystals. Silicon is a single crystal, but it was carefully aligned to the low-index zone axis.

IV. ANALYSIS AND DISCUSSION

The shape of the $1/\lambda(Z)$ dependence of Fig. 1 resembles (cf. Figs. 1 and 5) that of the mass density $\rho(Z)$. Therefore, in our preliminary study,[8] it was approximated as $1/\lambda \sim \rho^{0.3}$; however, no physical interpretation could be provided. In this section, we shall try to understand, at least qualitatively, the $1/\lambda(Z)$ variations of Fig. 1. We shall focus our discussion on the elemental solids and will briefly discuss the oxides in the end of the section.

Let us first discuss the dominant cause of inelastic scattering. In Introduction, it was suggested to be plasmons, however, Fig. 3 reveals it is not always the case. This complex figure presents the plasmon energy E_p and the energies of relevant core-loss transitions. The latter are conventionally labeled as M_{23}, M_{45}, N_{23}, N_{45}, N_{67}, O_{23}, and O_{45} and correspond to the transitions from the $3p$, $3d$, $4p$, $4d$, $4f$, $5p$, and $5d$ states to the excited state levels, respectively. Also shown

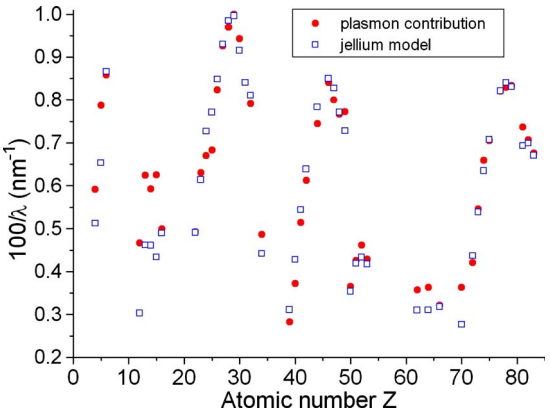

FIG. 4. (Color online) Solid circles show plasmon contribution to the inverse mean free path deduced for elemental solids from the data of Fig. 1. Open squares represent the fitting function $(\rho z/A)^{1/2}$ suggested by the jellium model.

in Fig. 3 are the characteristic EEL energies E_C, which in this work were calculated from the experimental spectra as

$$E_C^2 = \frac{\int S(E)EdE}{\int \frac{S(E)}{E}dE}. \quad (4)$$

Note that the function E_C is special by that it can be easily evaluated both experimentally and analytically.[1] For example, most other combinations of scattering functions do depend on the (plasmon) linewidth that brings extra complication to the analysis. On the contrary, within the jellium model, E_C is simply equal to E_p. Note, however, a noticeable difference between E_C and E_p in Fig. 3 which can be interpreted as follows.

In the light-element solids ($Z<20$), the core-loss energies are relatively large (hundreds of eV) and thus do not significantly affect the total EELS intensity. The scattering is dominated by plasmons, E_C is close to E_p, and their difference is due to the asymmetry of the plasmon peak, which is ignored in the free-electron model. For heavier elements, the contribution of the low-energy core-loss transitions becomes significant thus increasing the E_C-E_p difference. Note, however, that the largest difference is observed at $Z\sim 29$, 48, and 79 for elements with completed outer d shells, but those atoms do not show low-energy core-loss edges. This apparent inconsistency is discussed below (see Fig. 6), and it is argued that for those elements, no single plasmon energy can be defined, at least in terms of high-energy electron scattering.

The above discussion reveals that the ratio of the core-loss and plasmon contributions changes significantly with Z thereby complicating the analysis. In order to discuss the plasmon part only, we have removed the core-loss fraction and replotted the $1/\lambda(Z)$ data of Fig. 1 in Fig. 4. The removal procedure is discussed below (see Fig. 6). In order to provide clear reference data, we have also copied the λ values of Figs. 1 and 4 into Table I.

Figure 4 reveals that removing the core-loss component does not alter the shape of the $1/\lambda(Z)$ oscillations, but increases their amplitude. In attempt to fit their shape with the free-electron model [Eq. (1)], we have also plotted in Fig. 4 a $(\rho z/A)^{1/2}$ function. The fitting parameter was the number z of free electrons per atom, which was restricted to be equal to the number of either s or $s+p$ or $s+p+d$ electrons in the composite outer atomic shell. The latter includes the nd, $(n+1)s$, and $(n+1)p$ levels, $n=3,4,5$. They usually have close energies and therefore should be considered together. A reasonable agreement between the plasmon contribution and the $(\rho z/A)^{1/2}$ function is observed suggesting that the free-electron model can, at least qualitatively, explain the material dependence of the plasmon scattering.

Let us discuss z numbers, which were used for fitting the data of Fig. 4 and are summarized in Fig. 5. Values $z\leqslant 6$ correspond to the $s+p$ electrons. Larger z (up to 14) are, however, observed in Fig. 5 and originate from $s+p+d$ electrons in the outer shells. In order to understand such unusually large "valence" numbers, let us look back at the procedure, which we used to separate plasmon and core-loss contributions.

Figure 6 shows two representative cases: yttrium ($Z=39$, free-atom outer shell configuration of $5s^25p^1$, $z=3$) and palladium ($Z=46$, $4d^{10}$, $z=10$). The former example is representative of $z\leqslant 6$ cases. Here, plasmon and core-loss peaks can well be separated, for which we have used the following procedure: The high-energy tails of the EEL spectra were fitted with a polynomial function in materials with negligible core-loss contribution such as B, Be, P, S, and diamond. A characteristic function was found and applied to other materials. In most cases, however, only a small part of the plasmon spectrum could be used to adjust the fitting curve (see red line in the top part of Fig. 6) that brought extra uncertainty to the thus deduced plasmon contributions presented in Fig. 4 and Table I.

The palladium example is characteristic of $z\geqslant 6$ situation. Here, the plasmon peak ($\sim$8 eV for Pd) is accompanied by a number of other features; their separation can hardly be achieved unambiguously and therefore it has not been attempted. Those features probably correspond to different excitations of the composite outer shell consisting of different $4d+5s+5p$ electronic configurations. This interpretation suggests that the number of valence electrons per atom involved in plasmon scattering is larger than number of electrons taking part in chemical reactions.

In summary, the above analysis suggests that the periodic shape of the $1/\lambda(Z)$ dependence can well be explained by the combination of three major factors: mass density ρ, number of electrons z at the outer shell, and the core-loss transitions. In order to analyze their relative weights, we have plotted the corresponding values in Fig. 5 and found that those contributions to $1/\lambda$ are comparable: for example, elements from K ($Z=19$) to Ni ($Z=28$) show tenfold increase both in z (from 1 to 10) and ρ (0.89–8.9 g/cm^3) values. The core-loss fraction varies, but it can be $\sim$50% or larger for many materials.

Finally, as we have understood the $1/\lambda(Z)$ dependence in elemental solids, let us briefly discuss the oxides. Figure 1

TABLE I. Values of total mean free path (200 keV) of inelastic scattering λ and of plasmon contribution λ_P copied from Figs. 1 and 4. Accuracies are ~5%–10% for λ and ~10%–30% for λ_P.

Z	Material	λ (nm)	λ_P (nm)	Oxide	λ (nm)
4	Be	160	169		
5	B	123	126	B_2O_3	120
6	Diamond	112	116		
12	Mg	150	214	MgO	133
13	Al	134	160	Al_2O_3	140
14	Si	145	168	SiO_2	155
15	P	160	160		
16	S	200	200		
20				CaO	130
21				Sc_2O_3	125
22	Ti	120	202	TiO	120
23	V	109	158	V_2O_5	116
24	Cr	104	149	CrO_3	118
25	Mn	106	146		
26	Fe	102	121	Fe_2O_3	116
27	Co	98	108	CoO	115
28	Ni	98	103	NiO	115
29	Cu	100	100		
30	Zn	106	106	ZnO	117
31	Ga	110			
32	Ge	120	126	GeO_2	130
34	Se	130	205	SeO_2	135
38				SrO	126
39	Y	124	354	Y_2O_3	122
40	Zr	113	268	ZrO_2	115
41	Nb	105	194		
42	Mo	98	163	MoO_3	111
44	Ru	90	134		
46	Pd	94	118	PdO	110
47	Ag	100	125	Ag_2O	112
48	Cd	107	130		
49	In	110	129		
50	Sn	115	273	SnO_2	115
51	Sb	120	234		
52	Te	130	216	TeO_2	128
53	I	140	233		
56				BaO	125
57				La_2O_3	130
58				Ce_2O_3	125
59				Pr_2O_3	122
60				Nd_2O_3	120
62	Sm	112	280	Sm_2O_3	120
63				Eu_2O_3	118
64	Gd	110	275	Gd_2O_3	125
65				Tb_2O_3	125
66	Dy	118	310	Dy_2O_3	126
67				Ho_2O_3	120

TABLE I. (*Continued.*)

Z	Material	λ (nm)	λ_P (nm)	Oxide	λ (nm)
68				Er_2O_3	115
70	Yb	110	275	Yb_2O_3	115
72	Hf	95	237		
73	Ta	88	183	TaO	110
74	W	82	151	WO_3	110
75	Re	78	141		
77	Ir	78	121	IrO	110
78	Pt	82	120		
79	Au	84	120		
80				HgO	116
81	Tl	95	135		
82	Pb	99	141	PbO	122
83	Bi	105	147	Bi_2O_3	125

reveals much weaker Z dependence for the oxides that can be understood as follows. Introducing a fixed element oxygen into elemental solids results in averaging of the mean densities of atoms and valence electrons. For example, those densities decrease for transition metals and increase for alkali. This results in flattening of the $1/\lambda(Z)$ dependence in oxides, and we can anticipate a similar effect for other compounds (e.g., sulfides, nitrides, chlorides, etc.). Our experimental data support this intuitive suggestion, however, due to their major incompleteness, they are not presented here.

In the above paragraph, we have attempted to *qualitatively* explain the $1/\lambda(Z)$ variation in the oxides. It is possible to apply the *quantitative* analysis of the elemental solids, performed in this section, to the oxides. However, it would involve additional speculative quantities, such as average atomic and electronic densities, and therefore has not been attempted.

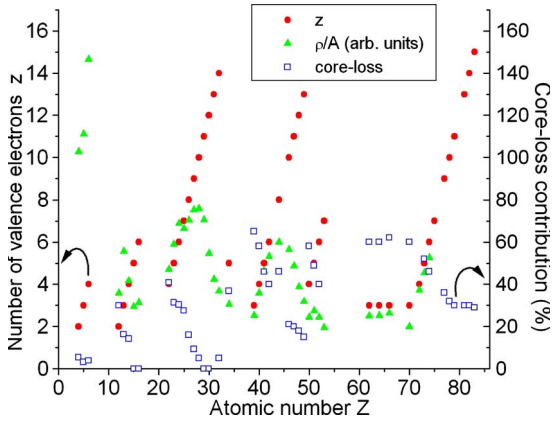

FIG. 5. (Color online) Relative contributions to the inverse mean free path data of Fig. 1 for elemental solids: number of valence electrons per atom z (solid circles), volume density of atoms ρ/A (solid triangles), and the core-loss fraction (open squares). All those contributions appear significant.

V. SUMMARY AND CONCLUSIONS

In this paper, we have reported the values of the mean free path λ of inelastic scattering for 200 keV electrons, systematically measured from most of the stable (ambient conditions) elemental solids and some oxides. The recently developed routine allowed us to increase the accuracy of measurements and consequently reveal a clear periodic dependence of λ as a function of atomic number Z, which was missed in the previous attempts[1,4,9] and which is the main achievement of this study. This $\lambda(Z)$ variation has not only academic but also practical value. In particular, our TEM observations (see Fig. 2) reveal its importance to the interpretation of bright-field TEM images.

In attempt to qualitatively explain the $\lambda(Z)$ dependence, we have split it up into the contributions of low-energy core-

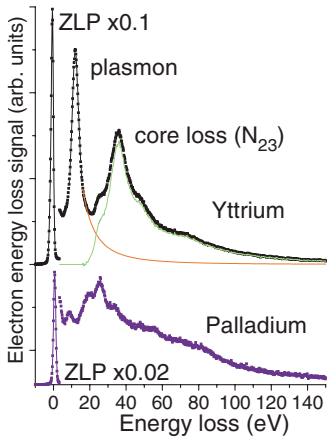

FIG. 6. (Color online) Two representative examples of separating the plasmon and core-loss contributions in the EEL spectra. ZLP marks the zero-loss electron scattering peak. The separation is rather straightforward for low-valence elements such as yttrium (upper spectrum), but not for elements with completed d shells, such as Pd (lower spectrum).

loss excitations and plasmons and analyzed the latter with the free-electron model. The $\lambda(Z)$ variation was explained by a product of three comparable factors, namely, atomic density ρ, number of "free" electrons per atom z, and the core-loss contribution.

An ambiguity of the EELS analysis has been revealed, such that the separation between the plasmon and low-energy core-loss transitions is hardly possible for transition metals with (nearly) filled outer d shell. This ambiguity probably originates not from imperfect mathematical procedures but from physical reasons—it may be argued that those elements not have a single plasmon peak, but a plasmon spectrum originating from various $d+s+p$ configurations of the outer shell.

ACKNOWLEDGMENTS

The authors are grateful to H. Shima and H. Akinaga (AIST, Tsukuba, Japan) for provision of the $Si/SiO_2/Ta/CoO/Pt$ and $Si/SiO_2/Ta/Pt/NiO/Al$ materials. This research was partially supported by Ministry of Education, Science, Sports, and Culture (MEXT) through the Grant-in-Aid for Young Scientists (B) 2005 17710120-6816 and the Nuclear Research Project.

*iakoubovskii.konstantin@nims.go.jp

[1] R. F. Egerton, *Electron Energy Loss Spectroscopy in the Electron Microscope* (Plenum, New York, 1986).
[2] H. Bethe, Ann. Phys. **5**, 325 (1930).
[3] C. J. Powell and A. Jablonski, J. Phys. Chem. Ref. Data **28**, 19 (1999).
[4] S. Tanuma, C. J. Powell, and D. R. Penn, Surf. Interface Anal. **25**, 25 (1997).
[5] M. Inokuti, J. L. Dehmer, T. Baer, and J. D. Hanson, Phys. Rev. A **23**, 95 (1981).
[6] F. Lenz, Z. Naturforsch. A **9A**, 185 (1954).
[7] A. Crewe, J. P. Langmore, and M. S. Isaacson, in *Physical Aspects of Electron Microscopy and Microbeam Analysis* (Wiley, New York, 1975).
[8] K. Iakoubovskii, K. Mitsuishi, Y. Nakayama, and K. Furuya, Microsc. Res. Tech. (to be published).
[9] P. A. Crozier, Philos. Mag. B **61**, 311 (1990).
[10] Y. Y. Yang and R. F. Egerton, Micron **26**, 1 (1995).
[11] R. F. Egerton and S. C. Cheng, Ultramicroscopy **21**, 231 (1987).
[12] Q. Jin, Microsc. Microanal. **10**, 882 (2004).
[13] O. L. Krivanek, C. C. Ahn, and G. J. Wood, Ultramicroscopy **33**, 177 (1990).
[14] R. Uemichi, Y. Ikematsu, and D. Shindo, J. Jpn. Inst. Met. **65**, 427 (2001).
[15] C.-W. Lee, Y. Ikematsu, and D. Shindo, J. Electron Microsc. **51**, 143 (2002).